Improved Stent Localization Using Shape-Based Similarity Scores

Rahmita Wirza O.K Rahmat, Farsad Zamani Boroujeni, Norwati Mustapha, Lilly Suriani Affendey
Faculty of Computer Science and Information Technology
Universiti Putra Malaysia
Selangor, Malaysia

Oteh Maskon
Department of Medicine
Universiti Kembangsaan Malaysia
Kuala Lumpur, Malaysia

Abstract— **Stent placement is a procedure to cure the narrowing of the coronary artery lumen due to plaque progression. In recent years, many solutions have been proposed on adopting computer assisted stent positioning systems for proper placement of the stent and apposition on the vessel wall. However, fast and accurate localization and tracking of the stents in conventional X-ray images is not sufficiently investigated in the literature. In this paper, a new method is proposed which is based on automatic detection of two radio-opaque landmarks of the stent. It improves the stent localization and tracking by filtering spurious markers and artifacts, causing a significant reduction in the number of outliers and misdetections. The validation results show that the proposed algorithm is suitable to be applied in routine clinical procedures.**

Keywords- coronary artery, guide-wire tracking, stent, X-ray imaging.

I. INTRODUCTION

Recently, there has been a great interest in incorporating tracking algorithms to improve guide-wire navigation and device localization during percutaneous transluminal coronary angioplasty. Generally, guide-wire tracking algorithms fall into two major categories. The first category involves implicit segmentation methods for estimating a probability of belonging to a linear segment for each pixel (e.g. pixel classification algorithms) followed by pixel grouping and segment ordering steps. The main objective of these methods is to delineate the whole guide-wire using low level operations such as edge detector filters [1], template matching [2], Vesselness measure [3, 4], AdaBoost pixel classification [5, 6] and many others.

The second category of methods aim at directly detecting the guide-wire using either a voting mechanism [7] or machine learning methods [8, 9]. The main idea is to develop a classifier to learn different patterns of guide-wire appearance and extract the matched objects from the image. However, it is observed that the difference between pose and scale of the learned patterns and image objects may hamper the process. On the other hand, the process of chaining the detected segment to obtain a complete guide-wire is often unsuccessful due to sensitivity of some methods to outliers and misdetections [2, 10]. Honnorat, et al. [5] presented a hierarchical grouping method to overcome the mentioned difficulties. They presented a pixel grouping and local and global segment ordering schema for perceptual organization of segments. Their experimental validation showed that their method is robust and efficient in extracting the guide-wire from fluoroscopic images. Nevertheless, the method only focused on segmentation purposes and its computational performance is not suitable for real-time tracking of the guide-wire which is indeed of great interest for device localization applications.

Some other methods in this category are based on local segmentation of therapeutic device (i.e. balloon or stent) through detecting the apparent features of the device (e.g. marker-balls) instead of segmenting the whole guide-wire or catheter. There has been a considerable interest on the segmentation of medical devices for endovascular interventions in both technical [11-16] and medical perspectives [17-19]. The enhancement methods focus on the improvement of the ability of an observer to detect guide-wire or therapeutic device in live image sequences. In a study conducted by Kompatsiaris, et al. [15], a method for extracting the stents in medical images was proposed. They focused on visibility of the stent after stent deployment in the angiographic images. Their method comprises of forming 3-D models of stents; deriving a set of 2-D models using perspective rules; matching said 2-D models with real-time angiographic images in a training phase; roughly detecting a stent in an angiographic image using a set of 2-D models and maximum likelihood criteria and refining the borders of the roughly detected stent using an active contour model. The problem with this method is that the computational burden of the algorithm makes it unsuitable for real-time implementation. Another related research work has been published without explanation of details and documented results [20]. They proposed a system for precise real-time localization of the stent and accurate device deployment during coronary device positioning. The method consisted of three main steps: 1) diagnostic stage for acquiring reference image data from a 3-D model and last injection image from the last sequence of contrast injection 2) guide-wire navigation which involves identification and tracking the balloon marker-balls using special preprocessing, correlation technique and motion consistency verification 3) Image registration wherein markers in current image and traced artery segment in reference image are translated to a vessel in the last injection image by employing ECG-gated frames.

978-0-7695-4959-0/13 $25.00 © 2013 IEEE
DOI 10.1109/ACSAT.2012.91

Finally, detected guide-wire or device is displayed on the 3-D reconstructed image. They also calculate some necessary parameters such as direction and curvature of the artery at guide-wire end point and local distance to bifurcation. However, in addition to tracking failures described by the author, their method requires pre-reconstruction of coronary vessel tree and acquisition of ECG-gated frames which are not always available in routine clinical procedures. In another discipline, Close, et al. [14] proposed a general framework for stent enhancement by motion layer decomposition. They assume that a single view X-ray image consists of several motion layers corresponding to different objects in the image. Having identified the motion of an object, the pixel intensity values of that motion layer can be estimated by a temporal averaging of the object's pixel values along the trajectory of the object. They reduced the problem of detecting the motion layer for the stent, to detecting the position of the stent marker-balls in the image sequence. Similarly, Florent, et al. [21] described an algorithm to enhance the stent through balloon marker-ball tracking with limited user interaction. Both methods only consider the marker-balls for estimating the motion of the stent which leads to misregisteration when the stent motions occur independently relative to the land mark motions. Bismuth, et al. [12] presented a non-linear registration approach to address the mentioned problem. Their registration method uses the segmented guide-wire between the marker-balls and apparent motion of the marker-balls to compute the motion field of the image area occupied by the stent. They demonstrated that employing the guide-wire joining the markers, significantly improves the quality of the stent image. However, their marker-ball detection process needs to be improved as it does not validate potential markers prior to building tracks of marker pairs and, therefore, the landmark detection process deals with a large number of outliers and misdetections.

This paper aims to propose a new marker-ball detection method for enhancing the accuracy of stent localization and tracking in fluoroscopic sequences. The method introduces a new technique for detection of stent-markers and filtering false and spurious marker-balls in a fluoroscopic image in order to track them in a frame sequence. The paper is organized as follows. Section II presents the proposed method. Section III, provides the results and discussion on the analysis of the algorithm's performance. Section IV concludes the paper.

II. The Proposed Method

The general solution to stent localization and tracking consists of four major steps as follows:

1. Detection of stent marker-balls in a single frame.
2. Filtering false detections and spurious marker-balls.
3. Object matching and data association analysis.
4. Tracking the stent marker-balls in a sequence of angiogram images.

The first step involves searching for spot-like objects that are likely to be one of the marker-balls in the angiogram and maintaining a set of candidate positions for each frame of the sequence. The second step is to filter out false detections (that are due to noise or image artifacts) by discarding unreliable candidates based on the appearance and intensity distribution of the candidate marker-balls. This results in reducing the search space and improving the performance of the tracking algorithm. The third step comprises of finding a marker-ball pair in the current frame that matches with the marker-ball pair found in the previous frame. Matching is performed based on several similarity measures and motion constraints such as the distance between the markers, proximity of the pairs and *a priori* knowledge of device. Once a pair of reliable markers is identified, the fourth step is to track them through the frame sequence. In the following sections we present those aspects of the stent localization approach necessary to marker-ball detection; we do not discuss the details of the object matching and tracking steps as they are previously described in the literature.

A. Detection of the Stent Markers

Fig. 1 shows an example fluoroscopic frame, acquired during the stent navigation procedure, which includes a catheter, a guide-wire and a stent which is indicated by its markers. As can be seen in the frame, the marker-balls occupy only a small part of the image, a very few suitable methods can be applied for stent marker-balls detection in fluoroscopic frame sequences. For tracking the small objects in the image, point representation is usually an appropriate method for object detection. Specifically, the solution is to consider the marker-balls as two local minima or local maxima points connected by their supporting guide-wire where each marker-ball can be represented by its local maxima pixel or centroid. This is close to the problem of detecting microcalcification spots in digital mammograms [22, 23]. Based on the spot detection methods, the marker-balls can be characterized by circular or elongated spots in the angiogram. Blostein and Ahuja [24] showed that Laplacian of Gaussian kernel (LoG) can be used to detect small spots if the size of the kernel is chosen appropriately.

The Laplacian kernel is obtained by calculating the second derivative of the 2-D Gaussian function:

$$LoG_{\sigma}(x,y) = -n(h)\frac{1}{\pi\sigma^4}\left(1-\frac{x^2+y^2}{2\sigma^2}\right)e^{-(x^2+y^2)/2\sigma^2} \quad (1)$$

where $h > 0$ denotes the scale of the filter in pixels which is defined as the diameter of the central lobe in the 2-D Laplacian filter and $-n(h)$ is the normalization factor to ensure that the response of the kernel is the same if the kernels with different scales are directly compared to each other [24]:

$$n(h) = \frac{1}{16}\, e\, h^2, \;\; h = 2\sqrt{2}\,\sigma \quad (2)$$

The scale-space convolution of the original image and the Laplacian kernel is defined as follows:

$$[LoG_h * f](x,y)\,, \qquad h = 1,2,\ldots,h_{max}. \quad (3)$$

For different scales of h, the size of the kernel is chosen to be $3h$ [25]. The examples of the mentioned normalized Laplacian filter kernels for different scales are shown in Fig. 2. The result of applying the LoG kernel to an image is a matrix (with the same size as the original image) in which every element represents the response value of the kernel at the corresponding image coordinate. By examining a large number of clinical sequences, it can be observed that the marker-balls are typically a pair of ellipses of large axis between 7 to 10 pixels in a given range of intensity values which make them differentiable from their surrounding area,

see Fig. 3. Therefore, a single scale of h=10 is selected for the LoG kernel, resulting a kernel of size 30x30 pixels.

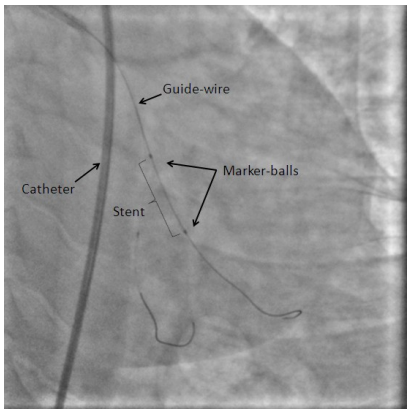

Fig. 1: A fluoroscopic frame (courtesy of UKM Medical Center, Malaysia) containing a catheter, a guide-wire and a stent with balloon marker-balls.

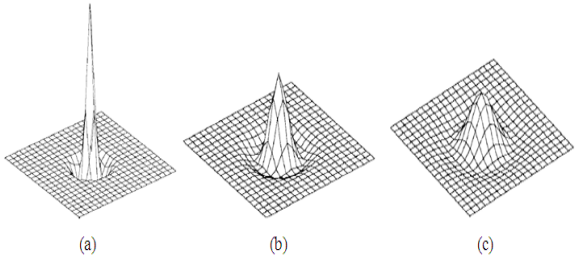

Fig. 2: Normalized Laplacian of Gaussian kernels for scales (a) $h = 3$ (b) $h = 5$ (c) $h = 7$.

In the next step, the response image is sought for local maxima locations in order to collect a set of candidate locations for the stent markers. Fig. 4 illustrates the local maxima locations after applying a 30x30 on an angiogram image.

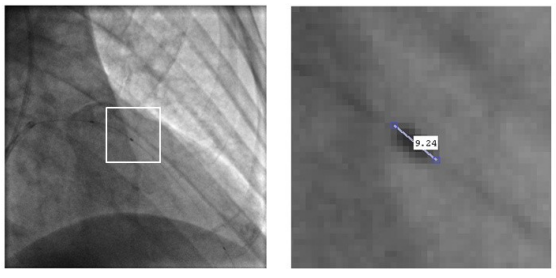

Fig. 3: (a) A frame selected from an angiogram sequence. (b) The magnified area of the white box shown in image a.

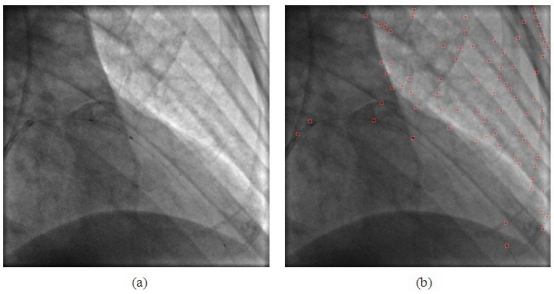

Fig. 4: The result of applying normalized Laplacian of Gaussian kernel on an example angiogram: (a) original image (b) local maxima points found on the filtered image which are indicated by squares.

B. Filtering False Detections and Spurious Marker-Balls

Certainly, the resulting image obtained by applying the *LoG* kernel contains many local maxima that do not correspond to stent marker-balls. Hence, discriminative features of marker-balls' appearance can be used to eliminate the false local maxima and reducing the search space for the tracking algorithm. In order to differentiate between the potential markers and false detections, the proposed idea is to segment the area of the original image that occupied by each local maxima point and its neighboring pixels within a particular neighborhood distance. Specifically, the pixels in the area are classified into object-pixels and background-pixels based in their intensity values using the automatic thresholding method proposed by Otsu [26]. The result is a circular binary image which represents the object-pixels on the local background. Fig. 5 illustrates a sample result of applying the proposed technique to different areas identified as local maxima points. It can be clearly seen that the pixels correspond to actual marker-balls tend to be centered and compact while the results correspond to the false detections exhibit sparse and decentralized patterns.

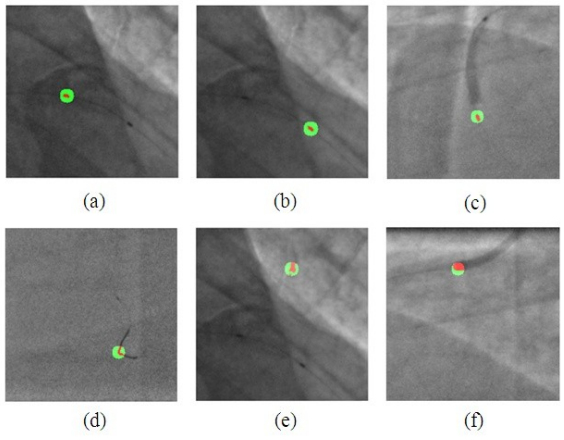

Fig. 5: The results obtained from applying the thresholding segmentation technique to local maxima points in different areas of the image. Images a, b and c show the segmentation result at actual marker-balls, while d, e and f show the segmentation results at false detections.

Several shape descriptors can be utilized as the measure of circularity or ellipticity of the segmented objects such as ratio of principal axes, convexity and compactness defined in [27] or moment invariants or elliptic variance suggested by [28]. In the fluoroscopic frames, the marker-balls are typically projected as an elliptic shape and it seems logical to use elliptic shape descriptors. However, due to the existence of outliers and in order to consider the distribution of the separateness of the segmented components, the compactness measure defined in [27] is utilized to validate the shape of the segmented object. According to their paper, the compactness measure is defined as:

$$Compactness = \frac{(perimeter\ of\ the\ object)^2}{area\ of\ the\ object} \quad (4)$$

It reaches the minimum of 2π in a circular object and approaches infinity in thin and complex objects. In the binary images, the perimeter is calculated as the number of pixels with value "1" that have at least one neighboring pixel with value "0". In our case, however, the compactness of an object is compared with a perfect circle, i.e. to calculate the compactness of the detected object with the area of A pixels, the ratio of the perimeter of a circle with the same area to the perimeter of the detected object is calculated:

$$Compactness\ Score = \frac{P_{circle}}{P_{object}} = \frac{2\pi\sqrt{A/\pi}}{P_{object}}, \quad (5)$$

where $A = A_{circle}$. Given a constant area A, the perimeter of a complete circle is always smaller than any other object. Therefore, the maximum value of the above compactness measure is 1 which is obtained when the detected object has circular shape and its minimum value approaches to 0 if the detected object has a complex and irregular pattern. It should be noted that this method does not take into account the size of the object. Therefore, a criterion of object size is also included in the shape validation process. By examination of several angiographic sequences, the average area occupied by the stent marker-balls in no-zoom angiograms and the corresponding standard deviation was measured and used to define the minimum and maximum threshold for validating the size of the detected object. Accordingly, the regions with areas smaller than the minimum threshold and larger than the maximum threshold are eliminated. According to the observations on our dataset, the minimum area of 20 pixels and the maximum area of 70 pixels are found to be suitable threshold values for the object size verification.

III. Results and Discussion

In the next, we conducted an experiment to verify the effectiveness of our approach. We are interested in evaluating how well the marker-ball filtering algorithm is capable of increasing the success rate of the detection algorithm by maintaining the correct markers and removing spurious objects over the fluoroscopic frame sequences. To this end, a ground truth dataset consisting of a large number of clinical image sequences (264 sequences acquired from 42 PCI examinations) is prepared. In each frame, the positions of the two marker-balls are marked by an operator so that the selected position lies inside the area occupied by the marker. However, since the exact location of the marker's centroid is unknown, a neighborhood distance of 5 pixels is defined as an acceptance range. An experiment was conducted to compare the position of the detected marker-balls with corresponding ground truth position on every frame. Having the ground truth and detected positions in hand, the success rate of the algorithm can be defined as:

$$SR = \frac{number\ of\ frames\ with\ successful\ detection\ of\ both\ markers}{total\ number\ of\ frames\ in\ the\ sequence} \quad (6)$$

The proposed marker-ball detection algorithm executed on the dataset and the above mentioned performance measure is computed for each image sequence. According to our observations over all sequences, the algorithm exhibits 87% reduction in the number of false detections before starting the object matching process. This results in significant improvement in the performance of the stent localization and tracking algorithm. Fig. 6 illustrates a histogram which contrasts the success rate of the algorithm in the case of merely using object matching and translation consistency criterion for marker-ball detection with the case in which the proposed filtering technique is used before the object matching step.

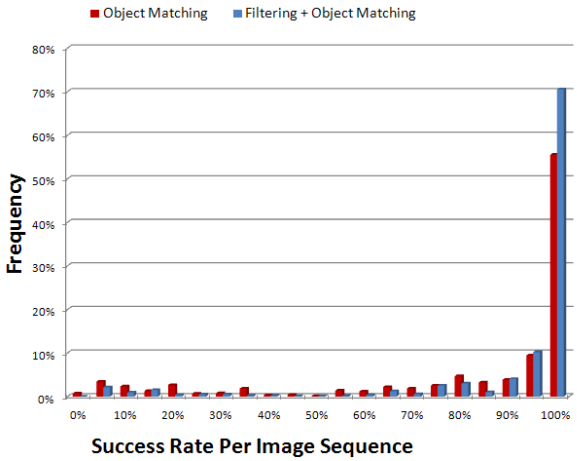

Fig. 6: The comparative success rate obtained from applying the proposed filtering technique before object matching process.

IV. Conclusion

In this study, we presented an efficient approach to stent localization and tracking through the detection of the stent landmarks in fluoroscopic frames. The proposed method incorporates shape-based information of marker pairs to identify a pair with consistent shape over the frame sequence. The most original contribution of the proposed method is the validation of the potential markers prior to building tracks of marker pairs which causes the landmark detection process to avoid dealing with a large number of outliers and misdetections. Performance validation results on a large number of clinical sequences showed that the proposed algorithm can be potentially applied in real-time stent positioning systems.

Acknowledgment

The authors wish to thank the medical staff of Cardiology Department in hospital HUKM Malaysia for their support in acquiring the sample images.

References:

[1] D. Palti-Wasserman, A. M. Brukstein, and R. P. Beyar, "Identifying and tracking a guide wire in the coronary arteries during angioplasty from x-ray images," *Biomedical Engineering, IEEE Transactions on,* vol. 44, pp. 152-164, 1997.

[2] S. A. M. Baert, M. A. Viergever, and W. J. Niessen, "Guide-wire tracking during endovascular interventions," *Medical Imaging, IEEE Transactions on,* vol. 22, pp. 965-972, 2003a.
[3] A. Frangi, W. Niessen, K. Vincken, and M. Viergever, "Multiscale vessel enhancement filtering," *Medical Image Computing and Computer-Assisted Interventation. MICCAI 98,* pp. 130-137, 1998.
[4] T. H. Heibel, B. Glocker, M. Groher, N. Paragios, N. Komodakis, and N. Navab, "Discrete tracking of parametrized curves," 2009, pp. 1754-1761.
[5] N. Honnorat, R. Vaillant, and N. Paragios, "Guide-wire extraction through perceptual organization of local segments in fluoroscopic images," *Medical Image Computing and Computer-Assisted Intervention, MICCAI 2010,* pp. 440-448, 2010b.
[6] F. Yoav and E. S. Robert, "A decision-theoretic generalization of on-line learning and an application to boosting," *Journal of Computer and System Sciences,* vol. 55, pp. 119-139, 1997.
[7] E. Franken, P. Rongen, M. van Almsick, and B. ter Haar Romeny, "Detection of electrophysiology catheters in noisy fluoroscopy images," *Medical Image Computing and Computer-Assisted Interventionâ€“MICCAI 2006,* pp. 25-32, 2006.
[8] A. Barbu, V. Athitsos, B. Georgescu, S. Boehm, P. Durlak, and D. Comaniciu, "Hierarchical learning of curves application to guide-wire localization in fluoroscopy," 2007, pp. 1-8.
[9] N. Honnorat, R. Vaillant, and N. Paragios, "Robust guide-wire segmentation through boosting, clustering and linear programming," 2010a, pp. 924-927.
[10] G. Slabaugh, K. Kong, G. Unal, and T. Fang, "Variational guide-wire tracking using phase congruency," *Medical Image Computing and Computer-Assisted Intervention, MICCAI 2007,* pp. 612-619, 2007.
[11] V. Bismuth and R. Vaillant, "A device enhancing and denoising algorithm for X-ray cardiac fluoroscopy," in *Pattern Recognition, 2008. ICPR 2008. 19th International Conference on*, 2008, pp. 1-4.
[12] V. Bismuth, R. Vaillant, F. Funck, N. Guillard, and L. Najman, "A comprehensive study of stent visualization enhancement in X-ray images by image processing means," *Medical Image Analysis,* 2011.
[13] R. A. Close, C. K. Abbey, and J. S. Whiting, "Improved image guidance of coronary stent deployment," in *Proceedings of SPIE*, 2000, pp. 301-304.
[14] R. A. Close, C. K. Abbey, and J. S. Whiting, "Improved localization of coronary stents using layer decomposition," *Computer Aided Surgery,* vol. 7, pp. 84-89, 2002.
[15] I. Kompatsiaris, D. Tzovaras, V. Koutkias, and M. G. Strintzis, "Deformable boundary detection of stents in angiographic images," *Medical Imaging, IEEE Transactions on,* vol. 19, pp. 652-662, 2000.
[16] J. Ross, D. Langan, R. Manjeshwar, J. Kaufhold, J. Manak, and D. Wilson, "Registration and integration for fluoroscopy device enhancement," *Medical Image Computing and Computer-Assisted Interventionâ€“MICCAI 2005,* pp. 851-858, 2005.
[17] D. S. G. Conway, W. H. T. Smith, J. Moore, and M. U. Sivananthan, "Measurement of coronary stent expansion using StentBoostTM image enhancement software: a comparison with intravascular ultrasound," *Brit. Heart J,* vol. 91, pp. A39-A40, 2005.
[18] J. Cordova, G. Aleong, H. Colmenarez, A. Cruz, E. Canales, P. Jimenez-Quevedo, R. Hernandez, F. Alfonso, C. Macaya, and C. Banuelos, "Digital enhancement of stent images in primary and secondary percutaneous coronary revascularisation," *EuroIntervention,* vol. 5, 2009.
[19] J. J. Koolen, M. Van het Veer, and C. E. Hanekamp, "StentBoost image enhancement: first clinical experience," *Medicamundi,* vol. 49, pp. 4-8, 2005.
[20] M. Zarkh and M. Klaiman, "Guide wire navigation and therapeutic device localization for catheterization procedure," 2005, pp. 311-316.
[21] R. Florent, L. Nosjean, P. Lelong, and P. M. J. Rongen, "Medical viewing system and method for enhancing structures in noisy images," ed: Google Patents, 2008.
[22] I. K. Cihan and H. G. Senel, "An Application of Topological Median on Detection and Clustering of Microcalcification in Digital Mammograms," 2006, pp. II-II.
[23] T. Netsch and H. O. Peitgen, "Scale-space signatures for the detection of clustered microcalcifications in digital mammograms," *Medical Imaging, IEEE Transactions on,* vol. 18, pp. 774-786, 1999.
[24] D. Blostein and N. Ahuja, "A multiscale region detector," *Computer Vision, Graphics, and Image Processing,* vol. 45, pp. 22-41, 1989.
[25] F. Neycenssac, "Contrast enhancement using the Laplacian-of-a-Gaussian filter," *CVGIP: Graphical Models and Image Processing,* vol. 55, pp. 447-463, 1993.
[26] N. Otsu, "A threshold selection method from gray-level histograms," *Automatica,* vol. 11, pp. 285-296, 1975.
[27] M. Peura and J. Iivarinen, "Efficiency of simple shape descriptors," 1997, pp. 443-451.
[28] P. L. Rosin, "Measuring shape: ellipticity, rectangularity, and triangularity," *Machine Vision and Applications,* vol. 14, pp. 172-184, 2003.
[29] Y. Xu, H. Zhang, H. Li, and G. Hu, "An improved algorithm for vessel centerline tracking in coronary angiograms," *Computer methods and programs in biomedicine,* vol. 88, pp. 131-143, 2007.
[30] S. R. Aylward and E. Bullitt, "Initialization, noise, singularities, and scale in height ridge traversal for tubular object centerline extraction," *Medical Imaging, IEEE Transactions on,* vol. 21, pp. 61-75, 2002.
[31] K. K. Delibasis, A. I. Kechriniotis, C. Tsonos, and N. Assimakis, "Automatic model-based tracing algorithm for vessel segmentation and diameter estimation," *Computer methods and programs in Biomedicine,* vol. 100, pp. 108-122, 2010.
[32] C. Biermann, I. Tsiflikas, C. Thomas, B. Kasperek, M. Heuschmid, and C. D. Claussen, "Evaluation of Computer-Assisted Quantification of Carotid Artery Stenosis," *Journal of Digital Imaging,* pp. 1-8, 2011.
[33] S. Mittal, Y. Zheng, B. Georgescu, F. Vega-Higuera, S. K. Zhou, D. Comaniciu, M. Kelm, A. Tsymbal, and D. Bernhardt, "Method and System for Automatic Detection and Classification of Coronary Stenoses in Cardiac CT Volumes," ed: Google Patents, 2011.